

A catalog of automatically detected ring galaxy candidates in PanSTARRS

Ian Timmis and Lior Shamir*

Lawrence Technological University, MI 48075

**email: lshamir@mtu.edu*

ABSTRACT

We developed and applied a computer analysis method to detect ring galaxy candidates in the first data release of PanSTARRS. The method works by applying a low-pass filter, followed by dynamic global thresholding to search for closed regions in the binary mask of each galaxy image. Applying the method to $\sim 3 \cdot 10^6$ PanSTARRS galaxy images produced a catalog of 185 ring galaxy candidates based on their visual appearance.

Subject headings: catalogs — techniques: image processing — methods: data analysis — galaxies: peculiar

1. Introduction

Ring galaxies are rare irregular galaxies that are not on the Hubble classifications scheme. Theys and Spiegel (1976) proposed a separate classification scheme for ring galaxies that includes three sub-classes based on their visual appearance: Empty ring galaxies (RE), Ring galaxies with off-center nucleolus (RN), and ring galaxies with knots or condensations (RK). They also identified that most, although not all, ring galaxies have a companion (Theys and Spiegel 1977). Few and Madore (1986) separated ring galaxies into two sub-classes: ‘P-type’ rings, which have a knotty structure or an off-center nucleolus, and ‘O-rings’, characterized by a

smooth ring structure and a centered nucleolus.

Ring galaxies can be identified as polar rings (Whitmore et al. 1990; Macciò et al. 2005; Reshetnikov and Sotnikova 1997; Finkelman et al. 2012; Reshetnikov and Combes 2015), collisional rings (Appleton and Struck-Marcell 1996), bar-driven or tidially-driven resonance rings (Buta 2000), ringed barred spiral galaxies (Buta et al. 2001) and Hoag-type objects (Longo et al. 2012). The ‘Hoag’s Object’ (Hoag 1950; Brosch 1985; Schweizer et al. 1987) was discovered in 1950, and its discovery was followed by the identification of other ring galaxies.

Catalogs of ring galaxies were created in the past by manual observation. The early

Arp (1966) catalog of peculiar galaxies contains two galaxies with visual appearance of an empty ring. The catalog of southern peculiar galaxies (Arp and Madore 1988) includes 69 systems identified as rings. Whitmore et al. (1990) compiled a list of 157 polar ring galaxy candidates, and about half a dozen of these objects were confirmed as polar ring galaxies by kinematic follow-up observations (Finkelman et al. 2012). Madore et al. (2009) prepared an atlas of collisional ring galaxies. Garcia-Ribera et al. (2015) discovered 16 polar ring galaxy candidates. Buta (1995) created a catalog of Southern ring galaxies. Moiseev et al. (2011) used crowdsourcing and non-scientists volunteers to prepare a catalog of ring galaxy candidates through the Galaxy Zoo citizen science campaign.

While manual analysis performed by expert or citizen scientists has provided useful catalogs of ring galaxies, the rapidly increasing data acquisition power of digital sky surveys such as the Large Synoptic Survey Telescopes (LSST) can potentially allow the identification of a very large number of ring galaxies among a total of billions of astronomical objects. Due to the large size of these databases, effective identification of these objects requires automation, leading to the development of automatic methods of identifying peculiar objects in large databases of galaxy images (Shamir 2012; Shamir and Wallin 2014; Shamir 2016). Here we describe an automatic image analysis method that can identify ring galaxies, and apply the method to mine through $\sim 3 \cdot 10^6$ galaxies imaged by the Panoramic Survey Telescope and Rapid Response System (Hodapp et al. 2004; Flewelling et al. 2016;

Chambers et al. 2016) to compile a catalog of ring galaxy candidates.

2. Methods

2.1. Data

The dataset was obtained from the Panoramic Survey Telescope and Rapid Response System (PanSTARRS) first data release (Hodapp et al. 2004; Flewelling et al. 2016; Chambers et al. 2016). The initial dataset includes 3,053,831 objects with r magnitude of less than 19. To avoid stars, the dataset included 2,394,452 objects identified as extended sources in all bands, and 659,379 additional objects that were not identified as extended objects in all bands, but their PSF i magnitude subtracted by their Kron i magnitude was larger than 0.05, and their r Petrosian radius was larger than 5.5". Objects that were identified as artifacts, has a brighter neighbor, defect, double PSF, or a blend in any of the bands were excluded from the dataset, as such objects require time to download and process while significantly increasing the false positive rate.

The images were then downloaded via the PanSTARRS *cutout* service as 120×120 JPG images, in a process similar to the image download done in (Kuminski and Shamir 2016). The JPG images that were downloaded and analyzed were the g band images, as the $y/i/g$ color images were in many cases noisy, and did not allow effective automatic analysis. To avoid pressure on the PanSTARRS web server, one image was downloaded at a time, and therefore the processes required 62 days to complete.

The initial scale was set to 0.25" per pixel. As done in (Kuminski and Shamir

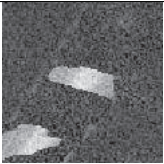
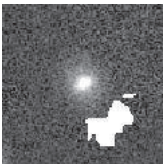
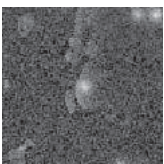



2016), after each image was downloaded, all pixels located on the edge of the frame with grayscale value higher than 125 were counted. If the number of these pixels was 25% or more of the total number of pixels on the edge the scale was increased by $0.05''$, and the image was downloaded again. That was repeated until the number of foreground pixels on the edge was lower than 25% of the total edge pixels. The change of the scale assisted in analyzing objects that are initially too large to fit in a 120×120 image of the initial $0.25''$ per pixel scale.

Images that contain substantial noise or artifacts are difficult to analyze correctly, and can trigger false positives as will be explained in Section 2.2. Due to the large scale of the initial dataset, even a low rate of false detections can lead to an unmanageable resulting dataset. Because compression algorithms are more efficient when the signal is smooth, clean images of real galaxies tend to have a smaller compressed file size, and therefore artifacts and noisy images can be rejected by their compressed file size (Kuminski and Shamir 2016). Table 1 shows examples of galaxy images and their file sizes. Based on empirical observations, a threshold was set so that only images with file sizes of less than 5.5KB were analyzed, and larger files were rejected.

2.2. Galaxy image analysis

Each image is smoothed by utilizing a median filter with window size of 5×5 to facilitate noise reduction, and converted to grayscale. The image is then converted into its binary mask using a dynamic threshold. The dynamic threshold starts with a minimum of 30, and is incre-

Table 1: Examples of clean galaxy images and artifacts or noisy images in PanSTARRS. The file size provides a simple mechanism to reject noisy images.

PanSTARRS object ID	File size (KB)	Image
102230806134866752	9.40	
103480451533225122	9.58	
103570759842751155	9.43	
100840464055080903	3.17	
104720155726185389	3.10	
104941422843081464	3.88	

mented iteratively until it reaches the gray level of 200. The conversion of the original ring galaxy into a binary map is displayed by Figure 1.

For each threshold level the binary mask

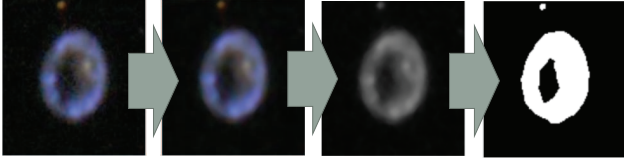


Fig. 1.— The stages in converting the original image into its binary map.



Fig. 2.— Dynamic thresholding binary maps. The Images show binary maps with thresholds of 20 (left), 44, 83, 99, and 115. The figure shows that when using a graylevel of 44 the ring is identified in the binary mask, while other graylevel thresholds show no ring.

is computed, and a search for a ring inside the foreground is done using a Flood Fill algorithm (Asundi and Wensen 1998). Flood fill is an algorithm typically associated with the “bucket fill” tool in painting programs. Here we used a stack-based 4-connected version of the flood fill algorithm, which is a non-recursive process starting with an initial pixel and then analyzes the four pixels surrounding it. Each of these four pixels is flagged, and then the neighbors of each of them are also added. That continues until all pixels are flagged, or no neighbors with value of 0 remain. In that case it is determined that no path of pixels of value 0 to the edge exist, and therefore the image is suspected as a ring galaxy. However, if a pixel that is on the edge of the image is flagged, the algorithm stops and it is determined that no ring exists in that graylevel threshold.

The flood fill algorithm is applied for each pixel in the binary mask. If the flood fill algorithm finishes without reaching a pixel that is on the edge of the frame, the number of pixels in the closed area are counted, and divided by the number of foreground pixels. If the number of pixels in the closed area is less than 10% of the number of foreground pixels, it is assumed that the closed area is too small to be considered a ring galaxy. Figure 3 shows an example of closed areas in the binary mask that can be considered candidate rings (left), and small areas in the binary mask of the same image that are merely local grayscale variations (right).



Fig. 3.— Comparison of the size of the closed area to the size of the foreground.

Processing of a small 120×120 galaxy image using a single core of an Intel Xeon E5-1650 requires ~ 2.1 seconds to complete.

2.3. False detections

When mining through a very large number of galaxies, even a small rate of false detections can lead to an unmanageable database. Of over three million images that were tested, the algorithm detected 2490 galaxies in which manual inspection showed no ring. These galaxies included artifacts, saturated objects, and regular galaxies. Figure 4 shows examples of false detections of the algorithm. As can be seen

in the example images, overlapping arms or stars nearby a spiral galaxy can lead to false detections. Saturated objects can also be mistakenly identified as rings. However, these objects are fairly rare, and the false detection rate is less than 0.1% of the initial set of galaxies.

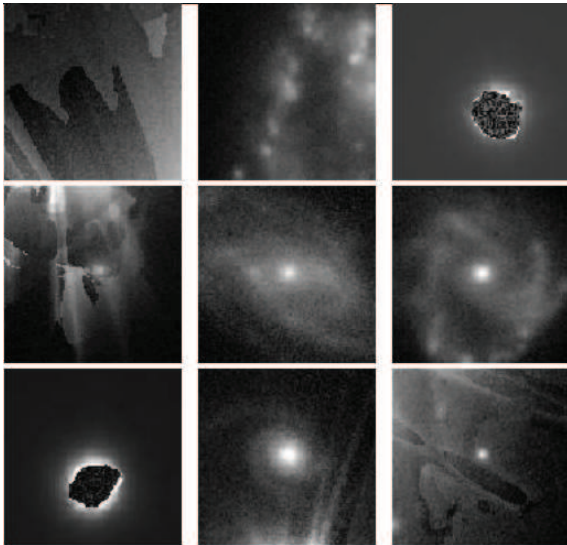


Fig. 4.— Examples of false detections of galaxies as rings

Another aspect related to false detection is confusion between ring galaxies and ringed disk galaxies (Buta 2013). That difference, however, is more difficult to identify automatically, as ringed disk galaxies feature ring-like structures, normally as nuclear, inner, or outer rings.

3. Ring galaxy candidates

The ring galaxy candidates that were detected with their right ascension and declination coordinates are shown in Table 2, ordered by the right ascension.

No.	Object ID	RA (°)	Dec (°)
1	102530019896912092	1.9897	-4.5569
2	98880036039558395	3.6039	-7.5933
3	135050044989180240	4.4989	22.5414
4	138120051156912877	5.1157	25.1019
5	72870063744005992	6.3744	-29.2703
6	120560064695882350	6.4696	10.4682
7	100400085662218636	8.5661	-6.3265
8	102310089038629907	8.9039	-4.7336
9	103950089186978353	8.9186	-3.3684
10	137290090541388746	9.0541	24.4152
11	115220097713265663	9.7715	6.0210
12	109660114619281831	11.4619	1.3845
13	111110125282677623	12.5283	2.5977
14	120890127618103802	12.7618	10.7444
15	92360151168438698	15.1168	-13.0264
16	119290184439583690	18.4440	9.4110
17	120590187339699694	18.7340	10.4993
18	105620208384294429	20.8384	-1.9799
19	112540211443478684	21.1444	3.7900
20	108010239026888389	23.9027	0.0150
21	130250272062931167	27.2063	18.5422
22	152300273312165338	27.3313	36.9206
23	136880303174084441	30.3172	24.0699
24	117300373539209184	37.3539	7.7573
25	144270387141449300	38.7141	30.2323
26	98420402083859546	40.2084	-7.9757
27	148070464186033529	46.4186	33.3941
28	102120545319045128	54.5319	-4.8960
29	89730546881066762	54.6881	-15.2197
30	105770557953197395	55.7953	-1.8525
31	94400582354418830	58.2354	-11.3263
32	98300585149137156	58.5149	-8.0777
33	103680672704100823	67.2704	-3.5997
34	87960731606800107	73.1606	-16.7
35	110590740360460369	74.0359	2.1585
36	93170740765876164	74.0766	-12.3534
37	90050743863589139	74.3863	-14.951
38	90040746028548781	74.6028	-14.9596
39	112280754250309794	75.4252	3.5745
40	108480776785245228	77.6784	0.4040

41	98820784238446846	78.4238	-7.6447
42	85450837400860065	83.74	-18.7919
43	77350864221236846	86.4221	-25.5362
44	179561088508306139	108.8508	59.6379
45	154011105647715883	110.5648	38.3460
46	194551123628248035	112.3629	72.1311
47	183491156027365911	115.6027	62.9125
48	151781161775920391	116.1776	36.4832
49	170881181537928277	118.1536	52.4061
50	164611201937762708	120.1938	47.1767
51	141001202112940207	120.2113	27.4997
52	133621235595071267	123.5595	21.3506
53	124791272138223104	127.2138	13.9938
54	171231275002484748	127.5002	52.6951
55	109361301796774389	130.1797	1.1367
56	190291319360661229	131.9360	68.5754
57	188281380666241185	138.0666	66.9
58	98371387382707506	138.7383	-8.0191
59	125181389138828530	138.9139	14.3234
60	130811416883240083	141.6883	19.0080
61	171161427964224003	142.7964	52.6361
62	82891436370344404	143.6370	-20.9216
63	94081470757770101	147.0758	-11.6001
64	123371475276486913	147.5276	12.8137
65	111101480001954462	148.0002	2.5867
66	154241493558096897	149.3558	38.5386
67	166351516903793594	151.6904	48.6275
68	107721522634947956	152.2635	-0.2271
69	141541526163197945	152.6163	27.9563
70	151261533456282945	153.3457	36.0520
71	181411561600712736	156.1601	61.1767
72	160351569982260063	156.9982	43.6245
73	123431607654498382	160.7655	12.8649
74	129391627135806697	162.7136	17.8302
75	76451645788803086	164.5791	-26.2894
76	98941648591968075	164.8592	-7.5435
77	153881653487717633	165.3487	38.2392
78	148781654085861195	165.4086	33.9839
79	168691656455379447	165.6455	50.5823
80	122761662462277308	166.2462	12.3057
81	167061663892379757	166.3893	49.2242
82	176441677887278299	167.7888	57.0397

83	177161677083354182	167.7084	57.6362
84	147611692157354849	169.2158	33.0119
85	169761694401977726	169.4402	51.4725
86	131551702348949298	170.2348	19.6322
87	83511707305532699	170.7306	-20.4065
88	132441708586612664	170.8587	20.3684
89	120061740415357108	174.0416	10.0555
90	145631743790845430	174.3791	31.3623
91	166121745010278457	174.5011	48.4398
92	103021750976199429	175.0976	-4.1425
93	140401760507263297	176.0507	27.0023
94	182681764076585291	176.4077	62.2371
95	171201764688293595	176.4689	52.6691
96	103361766457995817	176.6458	-3.8621
97	100891767811050892	176.7811	-5.9246
98	180361768453241219	176.8454	60.3004
99	81531787292064732	178.7292	-22.0546
100	146751794344735513	179.4344	32.2957
101	126861796962350039	179.6962	15.7163
102	120911807953598022	180.7954	10.7646
103	125491835740118715	183.5740	14.5818
104	121741853507871762	185.3508	11.4511
105	112761866548340926	186.6548	3.9671
106	137771871189921740	187.1190	24.8093
107	114301857795845888	185.7796	5.2545
108	125741873384637652	187.3385	14.7893
109	113901876468607202	187.6469	4.9223
110	144871915423938960	191.5421	30.7321
111	131131919673730819	191.9674	19.2752
112	152181932753561700	193.2755	36.8174
113	102921932899245357	193.2899	-4.2292
114	102271941347122534	194.1347	-4.7732
115	164961951082294851	195.1082	47.4702
116	119131965074384721	196.5074	9.2786
117	127841971925597729	197.1926	16.5394
118	102261975134478601	197.5134	-4.7764
119	107441989471515672	198.9471	-0.4623
120	105281992642316849	199.2642	-2.2613
121	95721996172550718	199.6172	-10.2331
122	133081997942710534	199.7943	20.9000
123	181722026514721806	202.6515	61.4342
124	174802054136252600	205.4136	55.6682

125	125292060017968309	206.0018	14.4148
126	103632081566171282	208.1566	-3.6409
127	127392083085689351	208.3086	16.1657
128	77702093105650034	209.3106	-25.2503
129	184722100380214976	210.0380	63.9369
130	112512111057222057	211.1057	3.7597
131	123332115027789738	211.5028	12.7828
132	123362118086413970	211.8086	12.8029
133	103052137786520187	213.7787	-4.1252
134	113472161524401485	216.1525	4.5592
135	109492177573061925	217.7573	1.2429
136	84542211439173056	221.1439	-19.5477
137	116152228525787253	222.8526	6.7973
138	183352242303877381	224.2304	62.7972
139	131032259389706416	225.9390	19.1966
140	148062302119596631	230.2120	33.3884
141	183392321197746552	232.1198	62.8298
142	148432328285931174	232.8286	33.6921
143	158172331153014314	233.1150	41.8113
144	148312333416204412	233.3416	33.5948
145	143522339208520736	233.9209	29.6001
146	129292352520407811	235.2520	17.7477
147	129462367458987309	236.7460	17.8890
148	202792388527621833	238.8528	78.9925
149	132902394059167588	239.4059	20.7559
150	131452396300467354	239.6301	19.5474
151	146322413429998230	241.3430	31.9397
152	110832424057543879	242.4057	2.3612
153	138262424254535667	242.4254	25.2209
154	108572432090906806	243.2091	0.4803
155	150852441278310269	244.1278	35.7081
156	144432453827808671	245.3828	30.3651
157	120402497965084423	249.7965	10.3366
158	164882506974275102	250.6974	47.4037
159	182962541826568261	254.1827	62.4729
160	137392563849799521	256.3850	24.4991
161	142632581066552766	258.1067	28.8602
162	178582585376172798	258.5377	58.8184
163	154302667799896469	266.7800	38.5882
164	162442713696719955	271.3698	45.3742
165	187092713680201538	271.3680	65.9089
166	180632732359767042	273.2359	60.5303

167	85913110560453012	311.0560	-18.4061
168	90603151049933857	315.1050	-14.4971
169	113963209792571680	320.9793	4.9677
170	102753218509133054	321.8509	-4.3728
171	121663222491624631	322.2492	11.3868
172	87453246504240833	324.6504	-17.1246
173	82723283048699480	328.3048	-21.0590
174	136183298529911556	329.8530	23.4842
175	82903312563109880	331.2564	-20.9087
176	131603342959906588	334.2960	19.6717
177	78253370037949323	337.0038	-24.7842
178	127173454713128088	345.4713	15.9813
179	124773504516095667	350.4516	13.9793
180	147543515744331454	351.5745	32.9506
181	102293536494361637	353.6494	-4.7573
182	132133578627738343	357.8628	20.1149
183	118623589791533531	358.9792	8.8525
184	136013594740073572	359.4740	23.3442
185	120513599153160081	359.9153	10.4247

Table 2:: Ring galaxy candidates identified automatically

| |

PanSTARRS images of the galaxies are displayed by Figures 5, 6, 7, and 8.

3.1. Comparison to Madore collisional ring Atlas

To assess the completeness of the catalog, the detected galaxies were compared to the Madore et al. (2009) catalog of collisional ring galaxies. The objects listed in Table 3 are objects from that catalog that are inside the footprint of PanSTARRS Data Release 1. The table shows the corresponding PanSTARRS object ID, and the Kron magnitude measured on the r band, which is used as a criteria for inclusion of objects in the initial dataset as described in Section 2. When multiple objects IDs are associated with the same extended source, the selected object ID is the object that its photometric information is the closest to the photometry threshold for selecting the objects as described in Section 2.1. The PSF i magnitude subtracted by the Kron i magnitude was also used as a method of filtering objects that are not galaxies, as well as the identification of the object as an extended sources in the g,r,i and z bands. When $i\text{PSFMag}-i\text{KronMag}$ is larger than 1000 it means that one of the $i\text{KronMag}$ reading was bad, leading to a -999 value. The table also shows what objects were detected as ring by the algorithm by downloading the image directly from PanSTARRS server and running the algorithm.

With the exception of NGC 4774, the objects are not included in Table 2. The reason for the exclusion of these objects from the catalog can be the inability of the algorithm to detect them, as in the case of Arp 145, Arp 146, NGC 985, and Arp 150.

Arp 145 is a relatively dim ring, and in the case of Arp150 and Arp 146 the ring is not full, and therefore the method failed to detect it due to an opening in the ring that allows the flood fill “escape” from the ring and reach the edge of the frame. These systems were included in the initial list of galaxies, but were not detected due to the inability of the method to detect them.

An interesting case is the object VII Zw 466, which was used as the object for demonstrating the algorithm in Section 2.2, but was not detected when applying the algorithm to the PanSTARRS images. The reason is that the PanSTARRS photometric object associated with it that was in the initial list is not the center of the ring, as shown by Figure 9. Because the object was not centered, the full ring was outside of the frame, and due to the few bright pixels on the frame the object was not identified as too large, and was therefore not re-scaled as described in Section 2.1.

The other objects were not included in the initial list of objects described in Section 2.1. For instance, Arp 318 is a group of “faint, diffuse streamers, peculiar galaxies” (Arp 1966), and as such is outside the scope of objects that can be identified by the algorithm described in Section 2. It also has bad $r\text{KronMag}$ measurement and was not detected as an extended source in any of the bands. Arp 10 also has bad $r\text{KronMag}$ measurement, and Arp 273 has bad $i\text{KronMag}$ measurement and was identified as an extended source only in two bands, and therefore did not meet the criteria for the initial list of galaxies described in Section 2.1. When testing the images, six out of the 17 systems were

Table 3: Collisional ring galaxies from (Madore et al. 2009) that are inside the footprint of PanSTARRS DR1.

Catalog name	PanSTARRS object ID	RA	DEC	Included in Table 2	r Kron magnitude	iKronMag-iPSFMag	extended source bands	Ring detected by the algorithm
Arp 146	100030016843707022	1.6841	-6.635	No	15.97	3.34	r,i,z	No
Arp 318	95800323797258621	32.379	-10.159	No	22.492	1022.611	–	n.a.
Arp 10	114770346040298405	34.609	5.653	No	-999	1020.9	–	Yes
Arp 273	155240353777382539	35.377	39.366	No	15.42	1021.098	g, r	No
Arp 145	157650357813012712	35.785	41.372	No	16.59	4.68	g,r,i,z	No
NGC 985	97450386522587254	38.657	-8.787	No	15.7	4.12	g,r,i,z	No
Arp 118	107770437986659641	43.795	-0.181	No	13.2	5.22	r,i,z	Yes
Arp 147	109570478265116474	47.829	1.315	No	16.89	0.86	r,i,z	No
Arp 219	105450549711618738	54.975	-2.118	No	17.14	3.8	r,i,z	Yes
Arp 141	196161085846518933	108.585	73.477	No	-999	1020.056	g	No
Arp 143	144021167270940513	116.723	30.019	No	20.18	0.98	g,r,i,z	No
NGC 2793	149311391915893056	139.197	34.430	No	-999	0	z	No
Arp 107	144071630704802930	163.069	30.065	No	16.87	3.8	r,i	No
Arp 148	157011659698568092	165.972	40.849	No	17.14	0	g,r	Yes
VII Zw 466	187681880151285551	188.018	66.404	No	16.76	2.73	g,r,i	Yes
NGC 4774	152191932750252225	193.275	36.823	Yes	15.459	1.7	g,r,i,z	Yes
Arp 150	119403498802526691	349.880	9.505	No	15.18	4.85	g,r,i,z	No

identified as rings by the algorithm. That shows that even if all PanSTARRS galaxies were tested, many more relevant system would still be hidden in the PanSTARRS database.

4. Conclusion

Autonomous sky surveys have enabled the acquisition of very large databases of image and other data, substantially increasing the discovery power of ground and space-based telescopes. To utilize the discovery power and turn these data into scientific discoveries, it is required to apply computational methods that can mine these very large databases. Since a substantial part of these data are in the form of images, full analysis of the data requires image analysis methodology. Here we use a simple and fast automatic image analysis method and apply it to the PanSTARRS first data release to detect ring galaxy candidates. Despite the simple nature of the

image analysis method, it can find ring galaxies that are highly difficult to find without using automation, and it is sufficiently fast to be applied to much larger databases such as LSST.

That shows that it is reasonable to assume that many more objects with ring structure could exist in PanSTARRS DR1, and were not detected in this experiment. Identifying all objects in PanSTARRS will require the improvement of the algorithm so that it can better handle “edge” cases, but also analysis of a larger dataset of PanSTARRS objects, as it is possible that many relevant objects did not meet the criteria for the initial data reduction. The PanSTARRS photometric pipeline can in some cases provide bad measurement values (e.g., “-999”) or fail to identify an extended source, leaving the object outside of the initial list of galaxies. The initial data reduction is required for reducing the very large PanSTARRS dataset of

over 3×10^9 objects to a “manageable” number of galaxies that can be downloaded and analyzed. Some objects such as Arp 138 are too large or have morphology that cannot be identified by the proposed algorithm. However, this study shows that applying a first step of automatic image analysis can identify objects that would require substantial labor to identify manually.

5. Acknowledgments

We would like to thank the anonymous reviewer for the insightful comments that helped to improve the manuscript. This study was supported by NSF grant IIS-1546079.

The Pan-STARRS1 Surveys (PS1) and the PS1 public science archive have been made possible through contributions by the Institute for Astronomy, the University of Hawaii, the Pan-STARRS Project Office, the Max-Planck Society and its participating institutes, the Max Planck Institute for Astronomy, Heidelberg and the Max Planck Institute for Extraterrestrial Physics, Garching, The Johns Hopkins University, Durham University, the University of Edinburgh, the Queen’s University Belfast, the Harvard-Smithsonian Center for Astrophysics, the Las Cumbres Observatory Global Telescope Network Incorporated, the National Central University of Taiwan, the Space Telescope Science Institute, the National Aeronautics and Space Administration under Grant No. NNX08AR22G issued through the Planetary Science Division of the NASA Science Mission Directorate, the National Science Foundation Grant No. AST-1238877, the University of Maryland, Eotvos Lorand University (ELTE), the Los Alamos Na-

tional Laboratory, and the Gordon and Betty Moore Foundation.

REFERENCES

- Appleton, P. and Struck-Marcell, C. (1996). Collisional ring galaxies. *Fundamentals of Cosmic Physics*, 16(111-220):18.
- Arp, H. (1966). Atlas of peculiar galaxies. *The Astrophysical Journal Supplement Series*, 14:1.
- Arp, H. C. and Madore, B. F. (1988). A catalogue of southern peculiar galaxies and associations. vol. i. positions and descriptions. *Contemporary Physics*, 29(1):99–102.
- Asundi, A. and Wensen, Z. (1998). Fast phase-unwrapping algorithm based on a gray-scale mask and flood fill. *Applied Optics*, 37(23):5416–5420.
- Brosch, N. (1985). The nature of hoag’s object—the perfect ringed galaxy. *Astronomy & Astrophysics*, 153:199–206.
- Buta, R. (1995). The catalog of southern ringed galaxies. *The Astrophysical Journal Supplement Series*, 96:39–116.
- Buta, R. (2000). Resonance rings and galaxy morphology. In *Toward a New Millennium in Galaxy Morphology*, pages 79–99. Springer.
- Buta, R., Ryder, S. D., Madsen, G. J., Wesson, K., Crocker, D., and Combes, F. (2001). Dynamics of ringed barred spiral galaxies. i. surface photometry and kinematics of ngc 1433 and ngc 6300. *The Astronomical Journal*, 121(1):225.

- Buta, R. J. (2013). Galaxy morphology. In *Planets, Stars and Stellar Systems*, pages 1–89. Springer.
- Chambers, K. C., Magnier, E., Metcalfe, N., Flewelling, H., Huber, M., Waters, C., Denneau, L., Draper, P., Farrow, D., Finkbeiner, D., et al. (2016). The pan-starrs1 surveys. *arXiv preprint arXiv:1612.05560*.
- Few, J. M. and Madore, B. F. (1986). Ring galaxies–ii. classification and statistics. *Monthly Notices of the Royal Astronomical Society*, 222(4):673–682.
- Finkelman, I., SJ, J. G. F., and Brosch, N. (2012). Polar ring galaxies in the galaxy zoo. *Monthly Notices of the Royal Astronomical Society*, 422(3):2386–2398.
- Flewelling, H., Magnier, E., Chambers, K., Heasley, J., Holmberg, C., Huber, M., Sweeney, W., Waters, C., Chen, T., Farrow, D., et al. (2016). The pan-starrs1 database and data products. *arXiv preprint arXiv:1612.05243*.
- García-Ribera, E., Pérez-Montero, E., García-Benito, R., and Vílchez, J. (2015). Initiating the sierra nevada catalogue of star-forming polar-ring galaxies. In *Highlights of Spanish Astrophysics VIII*, volume 1, pages 372–372.
- Hoag, A. A. (1950). A peculiar object in serpens. *The Astronomical Journal*, 55:170–170.
- Hodapp, K., Kaiser, N., Aussel, H., Burgett, W., Chambers, K., Chun, M., Dombeck, T., Douglas, A., Hafner, D., Heasley, J., et al. (2004). Design of the pan-starrs telescopes. *Astronomische Nachrichten*, 325(6-8):636–642.
- Kuminski, E. and Shamir, L. (2016). Computer-generated visual morphology catalog of $\sim 3,000,000$ sdss galaxies. *The Astrophysical Journal Supplement Series*, 223(2):20.
- Longo, G., Capaccioli, M., and Busarello, G. (2012). *Morphological and Physical Classification of Galaxies: Proceedings of the Fifth International Workshop of the Osservatorio Astronomico di Capodimonte*, volume 178.
- Macciò, A. V., Moore, B., and Stadel, J. (2005). The origin of polar ring galaxies: Evidence for galaxy formation by cold accretion. *The Astrophysical Journal Letters*, 636(1):L25.
- Madore, B. F., Nelson, E., and Petrillo, K. (2009). Atlas and catalog of collisional ring galaxies. *The Astrophysical Journal Supplement Series*, 181(2):572.
- Moiseev, A. V., Smirnova, K. I., Smirnova, A. A., and Reshetnikov, V. P. (2011). A new catalogue of polar-ring galaxies selected from the sloan digital sky survey. *Monthly Notices of the Royal Astronomical Society*, 418(1):244–257.
- Reshetnikov, V. and Combes, F. (2015). Polar-ring galaxies: the sdss view on the symbiotic galaxies. *Monthly Notices of the Royal Astronomical Society*, 447(3):2287–2294.
- Reshetnikov, V. and Sotnikova, N. (1997). Global structure and formation of polar-ring galaxies. *arXiv preprint astro-ph/9704047*.
- Schweizer, F., Ford Jr, W. K., Jedrzejewski, R., and Giovanelli, R. (1987).

The structure and evolution of hoag's object. *The Astrophysical Journal*, 320:454–463.

Shamir, L. (2012). Automatic detection of peculiar galaxies in large datasets of galaxy images. *Journal of Computational Science*, 3(3):181–189.

Shamir, L. (2016). Morphology-based query for galaxy image databases. *Publications of the Astronomical Society of the Pacific*, 129(972):024003.

Shamir, L. and Wallin, J. (2014). Automatic detection and quantitative assessment of peculiar galaxy pairs in sloan digital sky survey. *Monthly Notices of the Royal Astronomical Society*, 443(4):3528–3537.

Theys, J. and Spiegel, E. (1976). Ring galaxies. i. *The Astrophysical Journal*, 208:650–661.

Theys, J. C. and Spiegel, E. (1977). Ring galaxies. ii. *The Astrophysical Journal*, 212:616–619.

Whitmore, B. C., Lucas, R. A., McElroy, D. B., Steiman-Cameron, T. Y., Sackett, P. D., and Olling, R. P. (1990). New observations and a photographic atlas of polar-ring galaxies. *The Astronomical Journal*, 100:1489–1522.

This 2-column preprint was prepared with the AAS L^AT_EX macros v5.2.

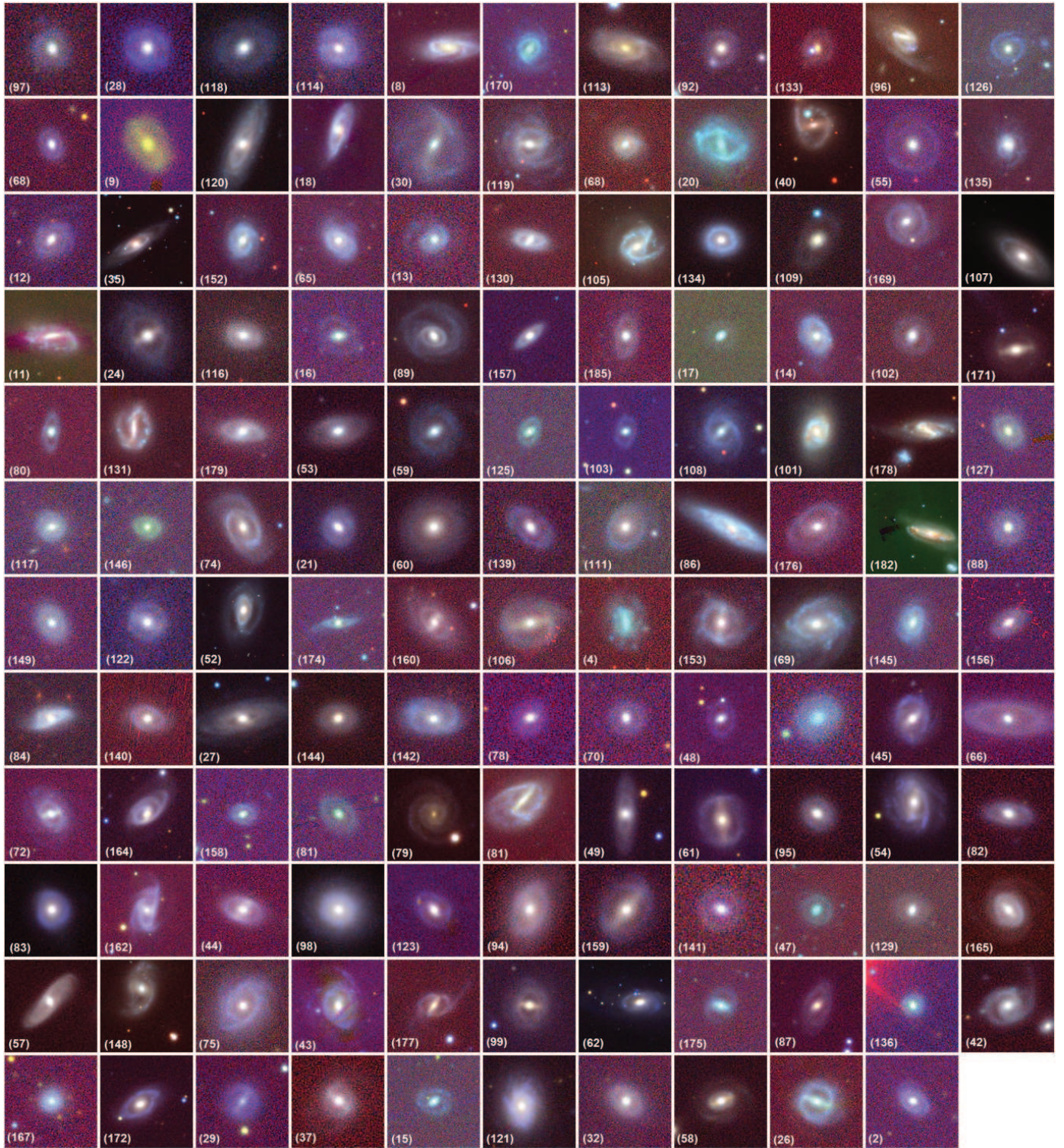


Fig. 5.— PanSTARRS images of resonance ring candidates in ordinary galaxies.

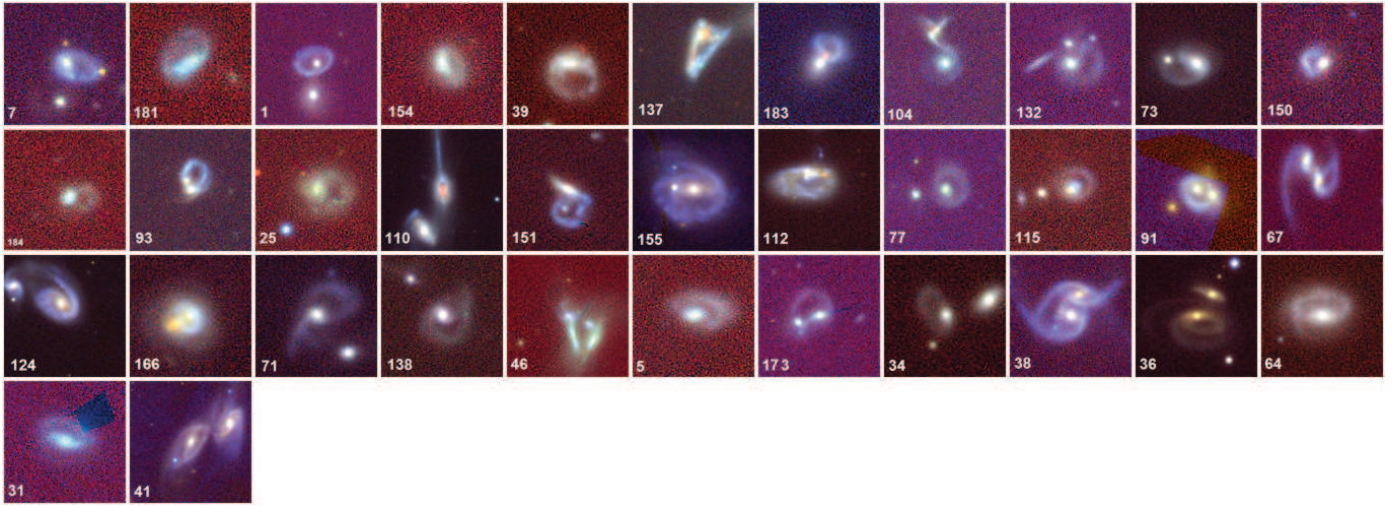


Fig. 6.— PanSTARRS images of collisional ring candidates.

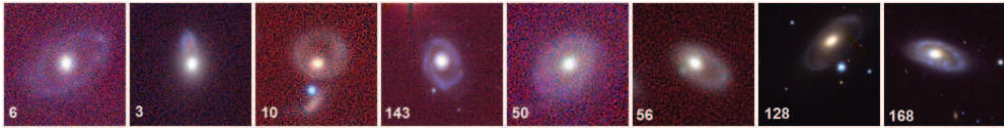


Fig. 7.— PanSTARRS images of ring galaxies with off-center nucleus.

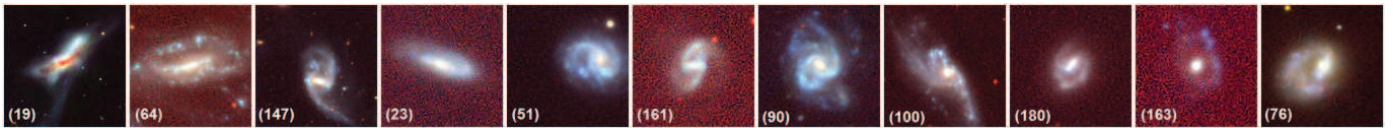


Fig. 8.— PanSTARRS images of other galaxies not included in Figures 5, 6, and 7.

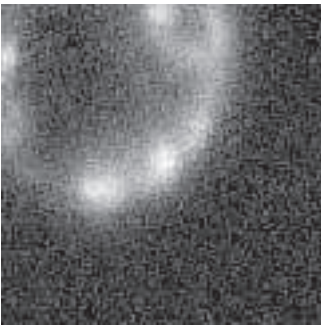


Fig. 9.— The 120×120 image of VII Zw 466 as downloaded for the initial list of galaxies described in Section 2.1